

Coherent Interference Fringes of Two-Photon Photoluminescence in Individual Au Nanoparticles: The Critical Role of the Intermediate State

Yao Li^{1,2,†}, Yonggang Yang^{1,2,†}, Chengbing Qin,^{1,*} Yunrui Song, Shuangping Han, Guofeng Zhang^{1,2}, Ruiyun Chen, Jianyong Hu, Liantuan Xiao,^{1,†} and Suotang Jia

State Key Laboratory of Quantum Optics and Quantum Optics Devices, Institute of Laser Spectroscopy, Shanxi University, Taiyuan, Shanxi 030006, China and Collaborative Innovation Center of Extreme Optics, Shanxi University, Taiyuan, Shanxi 030006, China



(Received 8 December 2020; accepted 21 July 2021; published 13 August 2021)

The interaction between light and metal nanoparticles enables investigations of microscopic phenomena on nanometer length and ultrashort timescales, benefiting from strong confinement and enhancement of the optical field. However, the ultrafast dynamics of these nanoparticles are primarily investigated by multiphoton photoluminescence on picoseconds or photoemission on femtoseconds independently. Here, we presented two-photon photoluminescence (TPPL) measurements on individual Au nanobipyramids (AuNP) to reveal their ultrafast dynamics by double-pulse excitation on a global timescale ranging from subfemtosecond to tens of picoseconds. Two orders of magnitude photoluminescence enhancement, namely, coherent interference fringes, has been demonstrated. Power-dependent measurements uncovered the transform of the nonlinearity from 1 to 2 when the interpulse delay varied from tens of femtoseconds to tens of picoseconds. We proved that the real intermediate state plays a critical role in the observed phenomena, supported by numerical simulations with a three-state model. Our results provide insight into the role of intermediate states in the ultrafast dynamics of noble metal nanoparticles. The presence of the intermediate states in AuNP and the coherent control of state populations offer interesting perspectives for imaging, sensing, nanophotonics, and in particular, for preparing macroscopic superposition states at room temperature and low-power superresolution stimulated emission depletion microscopy.

DOI: [10.1103/PhysRevLett.127.073902](https://doi.org/10.1103/PhysRevLett.127.073902)

Introduction.—Noble metal nanostructures have attracted much research interest in the past decades due to their localized surface plasmon resonance (LSPR), representing coherent collective oscillations of the conduction electrons [1,2]. This collective oscillation presents two intertwined features: subwavelength confinement of the optical field and thus giant enhancement of localized electric field [3,4], both of which are important for many promising applications, such as sensing [5,6], lasing [7,8], energy harvesting [9,10], and photothermal cancer therapy [11,12]. A significant research effort is currently focused on the coherent control of femtosecond energy localization in nanosystems by selectively exciting a number of eigenmodes of the metal nanoparticles through adaptive shaping of the laser pulse phase and amplitude [13–16]. However, full control of nano-optical fields is still challenging due to the complex dynamics of the system, which involves broad timescales from several femtoseconds to picoseconds [17–19]. Thus, exploring their ultrafast dynamics and understanding the relevant mechanisms are crucial for further applications.

Efforts toward the time-resolved measurements of metal-nanoparticles dynamics have involved two approaches. One investigated the dephasing processes on the timescale of several to tens of femtoseconds through traditionally

nonlinear interferometric autocorrelation (IAC) measurements. Experiments based on the high-order harmonic generation and multiphoton photoemission (MPPE) processes have been carried out [20–24]. According to the reconstructed plasmon-enhanced electric field $E(t)$ from these measurements, the pulse duration and thus the dephasing time can be derived. On the other aspect, the hot-carrier relaxation dynamics on the timescales of picoseconds have been studied by multiphoton photoluminescence (MPPL) [25–27]. The dynamics of metal nanoparticles have been severally performed through two individual approaches, and the corresponding ultrafast behaviors have been discussed independently. However, the global investigation, involving timescales from subfemtosecond to tens of picoseconds through the same approach, is highly desired to evaluate the unique phenomena and uncover the underlying mechanisms.

In this work, we address this limitation through two-photon photoluminescence (TPPL) measurements with a homemade Michelson interferometer by using ultrashort femtosecond laser pulses. Ultrafast dynamics of individual Au nanobipyramids (AuNP) on a global timescale—from subfemtosecond to tens of picoseconds—have been measured and analyzed. Almost 2 orders of magnitude photoluminescence (PL) enhancement, compared to traditional

TPPL, have been determined. We named this phenomenon coherent interference fringes. The nonlinearity orders of 2 have been determined for the global timescales when varying the total laser power. Interestingly, linear power-dependent behavior around zero interpulse delays was first obtained when changing the incident power of the first or second laser pulse. We have proved that the real intermediate state is critical for the exploring of coherent interference fringes and the linear optical behavior, which have been further supported by numerical simulations.

Results and discussion.—A schematic illustration of the experimental setup is depicted in Supplementa Material, Fig. S1 [28]. Particularly, individual rice-shaped AuNP with a diameter of 20 nm and length of 50 nm was used as a model to study the global ultrafast dynamics, benefiting from their high local field enhancement. A linear polarized femtosecond laser (15fs@800nm) was used to excite AuNP, where double pulse replicas with the time delay, Δt , were produced by a home-built Michelson interferometer. If not specified, the polarization of the double pulses was both along the long axis of AuNP (Fig. S3 [28]).

The typical MPPL trace of an individual AuNP as a function of interpulse delay has been illustrated in Fig. 1(a). At first glance, we can find the sharp and dramatic enhancement at $\Delta t \sim 0$, comparing with MPPL obtained by either single-pulse excitation or double-pulse excitation with sufficient long interpulse delay (for example, $\Delta t_{2PA} \sim 10$ ps, see follows for the significance of the subscript). To get insight into the detailed information, we plot the trace in logarithmic scale in Fig. 1(b). The double-pulse MPPL is twice that of the single-pulse excitation at the time delay of Δt_{2PA} . This result implies the coupling between the double pulses and the plasmon states of AuNP entirely vanishes. With the decrease of the interpulse delay, MPPL gradually increases. The change of MPPL in this process can be well fitted with a mono-exponential relationship. Here, we attributed this timescale (~ 1.46 ps) to the lifetime of intermediate states, τ_1 , which will be discussed later. When the interpulse delay is close to zero, almost 2 orders of magnitude enhancement of PL intensity, as compared to that of Δt_{2PA} , can be definitely determined. Simultaneously, the minimum PL intensity is close to zero (to background). Zooming in this area (the dashed rectangle), we can observe clear interference fringes, as shown in Fig. 1(c). To quantitatively describe the enhanced PL, we define an enhancement factor, that is, the ratio between the maximum PL intensity and that with sufficient long interpulse delays. For this AuNP, the enhancement factor is up to 102. This PL enhancement can be well reproduced on many AuNP in our experiment, with an averaged value to be 107 ± 12 (Fig. S4 [28]). We also proved that PL enhancement can be readily determined with orthogonal polarization, where the temporal and spectral interference effects of laser pulses have been excluded (Fig. S3 [28]). Thus, we address this giant enhanced MPPL as coherent interference fringes, originating from

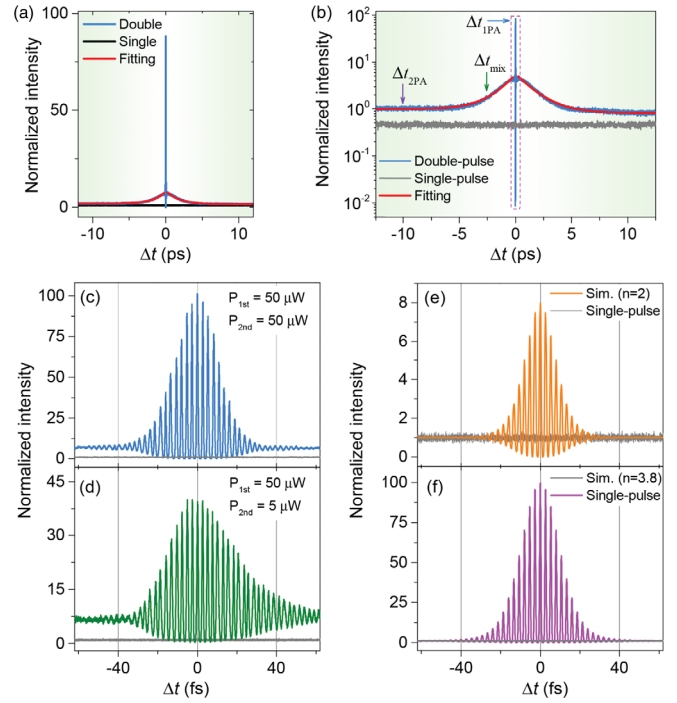


FIG. 1. Ultrafast dynamics of AuNP on global timescales. MPPL of AuNP as a function of interpulse delay (Δt) in the linear (a) and logarithmic plot (b). PL intensities are normalized by the intensity of double-pulse excitation with an interpulse delay of 10 ps. The solid red lines are the monoexponential fits with a lifetime of 1.46 ps. Δt_{IPA} , Δt_{2PA} , and Δt_{mix} represent three interaction regimes, which are one-photon absorption, two-photon absorption, and the mixed regime between them. The coherent interference fringes of experimental MPPL under equilibrium (c) and nonequilibrium (d) excitations. The powers of the first and second pulse have been marked in figures. Simulated MPPL with $n = 2$ (e) and $n = 3.8$ (f). The trace of single-pulse MPPL is also presented as a guide for eye.

the intrinsic features of AuNP. To our knowledge, these interference fringes have never been discussed conscientiously in the previous works. More intriguingly, as shown in Fig. 1(d), the interference fringes can be realized under the nonequilibrium excitation as well (the power ratio between the double pulses is in the region of 0.01–100, limited by the weak PL intensity and/or the irreversible damage under high power excitation, see Fig. S5 and S6 in the Supplemental Material for details [28]).

To date, the exact mechanisms of MPPL from Au nanoparticles are still in debated, either arising from the absorption of multiple photons through virtual or real intermediate states [19,25,29,30], or stemming from the emission process through intraband relaxation [27,29,31]. To explore the possible mechanism, we first assume that AuNP absorbs photons through virtual states. Thus MPPL can be treated as a quasi-instantaneous process. The signal of IAC (i.e., the MPPL intensity) can be given by $I^{AC}(\Delta t) = \int_{-\infty}^{+\infty} |E(t) + E(t - \Delta t)|^n dt$, with n being the order of nonlinearity [32,33]. Therefore, we

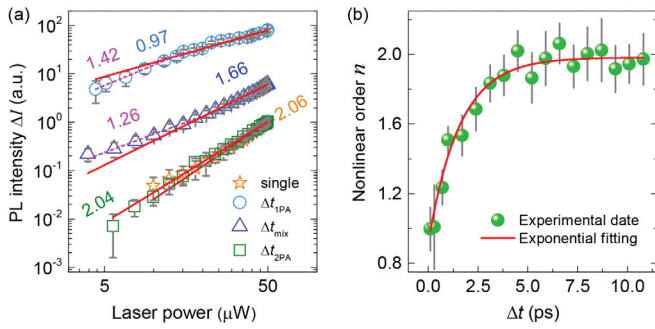


FIG. 2. Power-dependent TPPL behaviors on the global timescales. (a) Power dependence PL intensity for the single-pulse excitation and the double-pulse excitations for three dynamics regimes (taking $\Delta t_{1\text{PA}} = 0$ fs, $\Delta t_{\text{mix}} = 2.5$ ps, and $\Delta t_{2\text{PA}} = 10$ ps for examples). Here, the power of the first pulse was fixed at $50 \mu\text{W}$, while that of the second pulse was varying from 5 to $50 \mu\text{W}$. For two-pulse excitation, ΔI was determined by subtracting the background (excitation only by the first pulse) from the total intensity. The solid lines are the power-law fits, $\Delta I = a \times P^n$, with the exponents, n , presented in the figure. The short-dashed lines are the fits at low PL intensity (the power of the second laser was in the region of 5 to $20 \mu\text{W}$). (b) Power-law exponents for two-pulse excitation as a function of interpulse delay. The solid line represents the mono-exponential fits.

immediately simulate the interference fingers by assuming $n = 2$ according to the up-mentioned formula, as shown in Fig. 1(e). However, three intuitive facts illustrate the invalid of this simulation. First, the enhancement factor is 8, consistent with the feature of SHG [22,34–36] rather than close to a hundred. Second, simulated IAC persists for interpulse delays of less than 40 fs, rather than more than 60 fs for coherent interference fringes in our experiment (Fig. S7 [28]). Finally, PL decay at a longer timescale is absent. Outwardly, the simulation seems perfectly for constructive fringes with $n = 3.8$ [Fig. 1(f) and S8 of Ref. [28]]. However, the persistence of interference fringes and PL evolution as a function of time delay are still inconsistent with experiments. The difference between them further hints the presence of plasmon states and their relatively long dephasing time.

To undoubtedly determine the nonlinearity and the underlying mechanism of MPPL, we performed the power-dependent PL measurements at global timescales. We demonstrated $n = 2$ by synchronously varying the first and second laser power [Fig. S9 [28]] on the global timescales investigated, undoubtedly illustrating that the observed MPPL belongs to a two-photon process. However, as shown in Fig. 2(a), a novel result occurs when we explored the nonlinearity by fixing the power of the first (or second) pulse and varying the other one. We have proved that the nonlinearity is identical for both conditions (Figs. S10–S11 [28]). The nonlinearity is 2.06 for single-pulse excitation, coinciding with the second-order nonlinearity of TPPL. The nonlinear order at $\Delta t_{2\text{PA}}$ is

2.04, equals to single-pulse excitation, suggesting that the coupling between the two laser pulses and the plasmon states of AuNP entirely vanishes. Interestingly, when the interpulse is close to zero ($\Delta t_{1\text{PA}}$), the power-dependent TPPL approaches a linear behavior, with the nonlinearity to be 0.97. When the interpulse are between $\Delta t_{1\text{PA}}$ and $\Delta t_{2\text{PA}}$, the linear action and the two-photon process work together, presenting a regular change nonlinearity from 1 to 2, as illustrated in Fig. 2(b). More or less, these results agree with previous works on Au nanoantennas reported by Régis *et al.* [37]. However, some distinct features still declare the existence of hidden dynamics. (i) The nonlinearity of PL intensity is identical, either varying the power of the first pulse or changing that of the second pulse [37]. (ii) Next, the nonlinearity is strictly limited between 1 and 2. Higher nonlinearity orders are absent in our experiment [25,37]. (iii) At last, the nonlinearity as a function of interpulse delay follows a mono-exponential behavior [solid line shown in Fig. 2(b)], rather than the linear relationship published [29].

To interpret the coherent interference fringes as well as the power-dependent TPPL at the global timescale, we present a physical scenic that TPPL in AuNP arises from both one-photon (1PA) and two-photon absorption (2PA) involving the real intermediate states, as depicted in Fig. 3(a). Here we denote the ground, intermediate and excited states as $|0\rangle$, $|1\rangle$, and $|2\rangle$, respectively. After the first-pulse excitation, a few electrons will be pumped to excited states ($|2\rangle$) through 2PA, resulting in relatively weak TPPL. On the other aspect, vast electrons will be pumped to the intermediate state through 1PA due to their much larger absorption cross section. These electrons will be further excited to $|2\rangle$ to produce much stronger TPPL. However, they will relax to the ground state after excitation through the radiative and/or nonradiative process. Thus, the lifetime of the intermediate state (τ_1) can be determined by analyzing the TPPL as a function of interpulse delays, as the solid red lines shown in Fig. 1(b). We gain τ_1 to be 1.46 ps, close to the hot-carrier relaxation through carrier-photon interactions in the previous studies [19,37]. Specifically, these electrons will eventually lose the phase information because of the dephasing processes, such as electron-electron scattering and radiative damping. Within the dephasing time, these electrons can be coherently excited to the state $|2\rangle$ or recovered to the state $|0\rangle$, determined by the phase difference between the plasmon states and the second pulse. When the excited states are in phase with the second pulse, electrons arising from state $|1\rangle$ will be coherently excited to state $|2\rangle$ through farther 1PA and thus predominate TPPL. In this case, TPPL is dramatically enhanced than pure 2PA (i.e., the single-pulse excitation). The extra PL intensity results in the giant enhancement on interference fingers [Fig. 1(c)], compared to that obtained through virtual states [Fig. 1(e)]. Consequently, the power of the second pulse governs the intensity of TPPL, therefore displaying a linear power-dependent behavior. One may intuitively image the

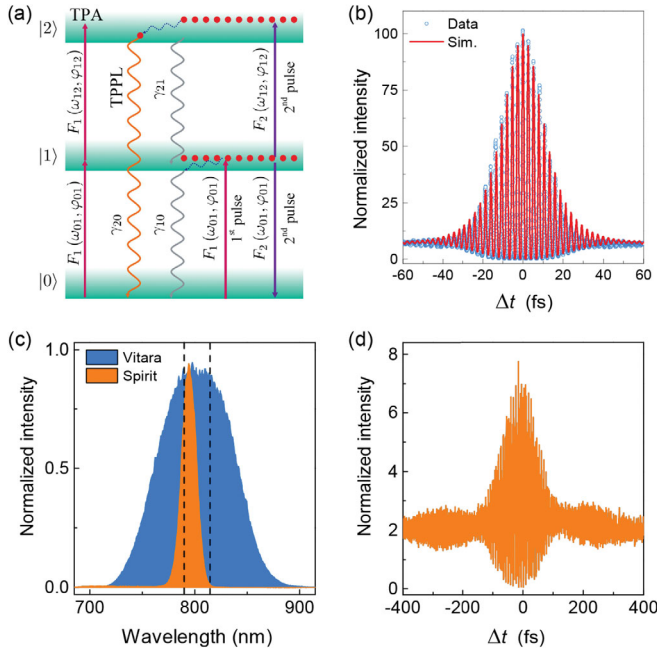


FIG. 3. Sketching energy levels of AuNP and numerical simulations. (a) Schematic of the energy levels of AuNP with real intermediate states. The resonant electric field of the first and second pulses denote as F_1 and F_2 , respectively. The solid and dashed wavy lines represent the radiative and relaxation processes. The red balls represent the excited electrons. TPA, two-photon absorption. (b) The experimental interference fringes and the corresponding numerical simulation. The parameters used for simulations can be found in Table I. (c) Spectral characteristics of the broadband (Vitara) and narrowband (Spirit) femtosecond laser. Two dashed lines highlight the resonant wavelengths [$c/(2\pi\omega_{01}) = 814$, $c/(2\pi\omega_{12}) = 792$ nm] for the simulation of interference in a. (d) Two-pulse excitation of the same AuNP using the narrowband laser (Spirit).

competition between 1 and 2PA, particularly under the nonequilibrium excitation. This can be proved by the departure of linear fit of Δt_{1PA} (the dashed lines) when the power of the second pulse was much lower than that of the first pulse. With the increasing of interpulse delays, the ratio of linear absorption (1 PA) decreases, and that of 2 PA increases, leading to an increase of nonlinear order, as shown in Fig. 2(b). As a consequent, we can classify the ultrafast dynamics of AuNP into three interaction regimes, that is, the one-photon absorption regime, the two-photon absorption regime, and the mixed regime between them, respectively, with t_{1PA} , t_{2PA} , and t_{mix} for short.

To prove our model and extract the ultrafast parameters of the three states as well as their couplings, we perform a numerical simulation to match the coherent interference fringes. The Hamiltonian of the AuNP can be written as $H_{NP} = \sum_e E_e |e\rangle\langle e| + \sum_v E_v |v\rangle\langle v| + \sum_{e'e''} \sum_{v'v''} g_{e'e''v'v''} |e\rangle |v\rangle\langle v'| \langle e''|$, where E_e and $|e\rangle$ are the eigenenergies and eigenstates of the electrons for the AuNP structure fixed at the equilibrium. E_v and $|v\rangle$ are the vibrational energies and states at the lowest electronic state. The states $|e\rangle |v\rangle$ form a

complete basis set for the Hamiltonian. As discussed above, the interaction between AuNP and the incident laser pulse $\vec{F}(t)$ can be characterized as $H_{int} = -\vec{\mu} \cdot \vec{F}(t)$. For the double-pulse excitation, $\vec{F}(t)$ has the form of $\vec{F}(t) = \vec{F}_1(t) + \vec{F}_2(t + \Delta t)$, where the electric field of each pulse is approximated as $\vec{F}_k(t) = \vec{F}_0 \cdot e^{-t^2/\tau_0^2} \cdot \sin(\omega_0 t)$ for $k = 1, 2$. Both the first and second pulses have Gauss envelope, with the pulse duration τ_0 and central frequency ω_0 , respectively [in our experiment $\tau_0 = 15$ fs; $c/(2\pi\omega_0) = 800$ nm].

The total Hamiltonian is then $H = H_S + H_B + H_{S-B}$. The system Hamiltonian involving the laser pulses and the three states is characterized as $H_S = \sum_{n=0}^2 E_n |n\rangle\langle n| - \sum_{nn'} \vec{\mu}_{nn'} \cdot \vec{F}(t) |n\rangle\langle n'|$. The other relevant states are described as bath degrees of freedom with energies E_b and states $|b\rangle$. The Hamiltonian of the bath (H_B) and its interaction with the system are given by $H_B = \sum_b E_b |b\rangle\langle b|$ and $H_{S-B} = \sum_{nb} (t_{nb} |n\rangle\langle b| + t_{nb}^* |b\rangle\langle n|)$, respectively. The quantum state of the system can be characterized by the density operator $\rho(t) = \sum_{nn'} \rho_{nn'}(t) |n\rangle\langle n'|$. The propagation of the density operator obeys the quantum master equation $(\partial/\partial t)\rho(t) = (1/i\hbar)[H_S, \rho(t)] - \mathfrak{R}\rho(t)$. Here \mathfrak{R} is the dissipation super-operator defined in terms of several dephasing or relaxation rates $\Gamma_{nn'}$ as $\mathfrak{R}_{nn',mm'} = \delta_{nm}\delta_{n'm'}\Gamma_{nn'}$. The physical meaning of each $\Gamma_{nn'}$ is transparent. Specifically, Γ_{22} is the sum of the bath-induced population transfer rate from $|2\rangle \rightarrow |1\rangle$ (γ_{21}) and the one from $|2\rangle \rightarrow |0\rangle$ (γ_{20}); while Γ_{11} means the difference between the population transfer rate from $|1\rangle \rightarrow |0\rangle$ (γ_{10}) and the one from $|2\rangle \rightarrow |1\rangle$ (γ_{21}). The off-diagonal $\Gamma_{nn'}$ means bath-induced dephasing rate of the coherence between states $|n\rangle$ and $|n'\rangle$. The initial condition of the quantum state is $\rho_{nn'}(t = -\infty) = \delta_{n0}\delta_{n'0}$. In the numerical simulations, the density matrix is normalized at each time step to ensure the conservation of probability $\sum_{n=0}^2 \rho_{nn}(t) = 1$.

TPPL intensity is proportional to the population of the state $|2\rangle$, namely, $\rho_{22}(t)$. Note, according to the lifetime of the intermediate state, the values of $\hbar\gamma_{21}$ and $\hbar\gamma_{10}$ are basically in the same magnitude as 2.83 meV (1.46 ps). To reach an acceptable match of both interference fingers and enhanced TPPL beyond interference, two different frequencies [$c/(2\pi\omega_{01}) = 814$ and $c/(2\pi\omega_{12}) = 792$ nm] are needed to couple the transition of $|0\rangle \rightarrow |1\rangle$ and $|1\rangle \rightarrow |2\rangle$, hinting two-color two-photon absorption. That is, broadband excitation is needed to prepare the coherent superposition states and to achieve coherent interference fringes. To verify this conclusion, we excite the same AuNP using a narrowband femtosecond laser [Fig. 3(c), Spirit, Spectra-Physics]. The center wavelength is also 800 nm with pulse width of 80 fs. The result is presented in Fig. 3(d). We can find that the enhancement factor is close to 7, much smaller than that of broadband excitation (107 ± 12). This result indicates that only a few vibrational

modes associated with the resonant interference, and thus most of TPPL intensity was originating from the nonresonant two-photon excitation. This conclusion can be further supported by the diminished PL enhancements under the narrowband excitation with the center wavelength varying from 790 to 860 nm (Fig. S12 [28]). Therefore, we can expect that a shorter laser pulse is crucially beneficial for the preparation of coherent interference fringes. Additionally, the value of $\hbar\Gamma_{02}$ can be inspired by previous works involving dephasing studies [22,35]. With these choices, the simulated result agrees fairly well with the experiment, as shown in Fig. 3(b) (Fig. S8 shows simulations with the timescales of 10 ps [28]). The used parameters listed in Table S1 coincide with the relevant reports. Moreover, the dephasing rate $\hbar\Gamma_{02}$ of 349 meV (11.9 fs) agrees well with the plasmon dephasing rate of similar Au nanoparticles [22,35].

To shed more light on the details of intermediate states and their critical roles on the coherent interference fringes, we further studied the size-dependent TPPL on Au nanospheres (AuNS) with diameters ranging from 20 to 160 nm (Fig. S13–14 [28]). The corresponding parameters are listed in Table S1 [28]. Among these parameters, the change of $\hbar\Gamma_{01}$ ($\hbar\Gamma_{12}$) and $\hbar\Gamma_{22}$ is more significant, implying shorter dephasing time between the relevant states in larger AuNS. The variations of these parameters are in accord with the increase of their vibrational modes. The well reproducible coherent interference fringes on different Au nanomaterials pursue a wide variety of applications. For examples, the coherent control of states population offers an excellent method to prepare macroscopic superposition at room temperature under atmosphere environment, rather than cryostatic conditions under high vacuum previously [38–40]. Furthermore, the nonequilibrium coherent interference fringes [Fig. 1(d) and Fig. S5 [28]] indicates that strong TPPL can be readily established through the first pulse excitation with high power, and TPPL can be fully quenched through stimulated emission by the second pulse with extremely low power. The feature provide a great opportunity to realize low-power superresolution stimulated emission depletion (STED) microscopy [41], overcoming the requirement of high laser power in STED which can cause photobleaching and phototoxicity [42,43].

Conclusion.—In summary, we have proved, based on the TPPL experiments on the timescales from sub-femtosecond to tens of picoseconds and numerical simulations with a three-state model, the critical role of the intermediate state for the coherent interference fringes in individual AuNP. We presented that TPPL can be enhanced by almost two orders of magnitude by two-pulse broadband resonant coherent excitation, compared to that excited by single pulse. We also demonstrated that ultrafast dynamics and power-dependent TPPL of AuNP manifested complicated but regular behaviors with the change of interpulse delays. By considering the presence of the intermediate state and its dephasing process, all the experimental results can be

well explained and simulated. We also proved the same results on the AuNS with different diameters. Our finding suggests that the intermediate state dominates TPPL under double-pulse excitation and enables dramatic PL enhancement, highlighting great importance both for basic science experiments and potential practical applications in optoelectronics, such as preparation of macroscopic superposition and implementation of superresolution imaging.

The authors gratefully acknowledge support from the National Key Research and Development Program of China (Grant No. 2017YFA0304203), Natural Science Foundation of China (No. 91950109, No. 61875109, No. 61527824, No. 61675119, and No. 62075122), Natural Science Foundation of Shanxi Province [No. 201901D111010 (Z. D.)], PCSIRT (No. IRT_17R70), 111 projects (Grant No. D18001), 1331KSC, and PTIT. C. Q. and L. X. designed and supervised the experiments. Y. L., Y. S., and S. H. carried out the optical experiments. Y. Y. and Y. L. performed the numerical simulations. G. Z., R. C., and J. H. prepared and characterized the sample. X. L., C. Q., Y. L., and Y. T. wrote the manuscript. All authors commented on the manuscript.

The authors declare no competing interests.

*Corresponding author.
chbqin@sxu.edu.cn

†Corresponding author.
xlt@sxu.edu.cn

‡These authors contributed equally to this work.

- [1] S. K. Ghosh and T. Pal, *Chem. Rev.* **107**, 4797 (2007).
- [2] K. M. Mayer and J. H. Hafner, *Chem. Rev.* **111**, 3828 (2011).
- [3] P. Y. Hou, Y. Y. Huang, X. X. Yuan, X. Y. Chang, C. Zu, L. He, and L. M. Duan, *Nat. Commun.* **7**, 11736 (2016).
- [4] M. S. Tame, K. R. McEney, Ş. K. Özdemir, J. Lee, S. A. Maier, and M. S. Kim, *Nat. Phys.* **9**, 329 (2013).
- [5] A. B. Taylor and P. Zijlstra, *ACS Sens.* **2**, 1103 (2017).
- [6] K. Saha, S. S. Agasti, C. Kim, X. Li, and V. M. Rotello, *Chem. Rev.* **112**, 2739 (2012).
- [7] A. K. Yang, T. B. Hoang, M. Dridi, C. Deeb, M. H. Mikkelsen, G. C. Schatz, and T. W. Odom, *Nat. Commun.* **6**, 6939 (2015).
- [8] R. Chandrasekar *et al.*, *ACS Photonics* **4**, 674 (2017).
- [9] S. Linic, P. Christopher, and D. B. Ingram, *Nat. Mater.* **10**, 911 (2011).
- [10] A. Kubacka, M. Fernandez-Garcia, and G. Colon, *Chem. Rev.* **112**, 1555 (2012).
- [11] S. Hwang, J. Nam, S. Jung, J. Song, H. Doh, and S. Kim, *Nanomedicine* **9**, 2003 (2014).
- [12] R. Han *et al.*, *ACS Nano* **14**, 9532 (2020).
- [13] M. Aeschlimann, M. Bauer, D. Bayer, T. Brixner, F. J. Garcia de Abajo, W. Pfeiffer, M. Rohmer, C. Spindler, and F. Steeb, *Nature (London)* **446**, 301 (2007).
- [14] C. Forestiere, G. Miano, M. Pascale, and R. Tricarico, *Phys. Rev. A* **102**, 043704 (2020).
- [15] L. Michaeli, S. Keren-Zur, O. Avayu, H. Suchowski, and T. Ellenbogen, *Phys. Rev. Lett.* **118**, 243904 (2017).

- [16] G.-F. Jiao, K. Zhang, L. Q. Chen, W. Zhang, and C.-H. Yuan, *Phys. Rev. A* **102**, 033520 (2020).
- [17] E. Marsell *et al.*, *Nano Lett.* **15**, 6601 (2015).
- [18] P. Ruello, A. Ayouch, G. Vaudel, T. Pezeril, N. Delorme, S. Sato, K. Kimura, and V. E. Gusev, *Phys. Rev. B* **92**, 174304 (2015).
- [19] X. F. Jiang, Y. Pan, C. Jiang, T. Zhao, P. Yuan, T. Venkatesan, and Q. H. Xu, *J. Phys. Chem. Lett.* **4**, 1634 (2013).
- [20] A. Grubisic, V. Schweikhard, T. A. Baker, and D. J. Nesbitt, *ACS Nano* **7**, 87 (2013).
- [21] G. Herink, D. R. Solli, M. Gulde, and C. Ropers, *Nature (London)* **483**, 190 (2012).
- [22] B. Lamprecht, A. Leitner, and F. R. Aussenegg, *Appl. Phys. B* **68**, 419 (1999).
- [23] M. Wu, J. Jean, V. Bulović, and M. A. Baldo, *Appl. Phys. Lett.* **110**, 211101 (2017).
- [24] T. Hanke, G. Krauss, D. Trautlein, B. Wild, R. Bratschitsch, and A. Leitenstorfer, *Phys. Rev. Lett.* **103**, 257404 (2009).
- [25] O. Demichel, M. Petit, S. Viarbitskaya, R. Méjard, F. de Fornel, E. Hertz, F. Billard, A. Bouhelier, and B. Cluzel, *ACS Photonics* **3**, 791 (2016).
- [26] R. Hernandez, R. Juliano Martins, A. Agreda, M. Petit, J.-C. Weeber, A. Bouhelier, B. Cluzel, and O. Demichel, *ACS Photonics* **6**, 1500 (2019).
- [27] K.-Q. Lin, J. Yi, S. Hu, J.-J. Sun, J.-T. Zheng, X. Wang, and B. Ren, *ACS Photonics* **3**, 1248 (2016).
- [28] See Supplemental Material at <http://link.aps.org/supplemental/10.1103/PhysRevLett.127.073902> for the supporting information includes experimental details; coherent interference fringes under equilibrium, and non-equilibrium excitation; Comparison between one-and two-photon excitation, experiments, and simulations; Irreversible PL behaviors under high power excitation; the nonlinearity of MPPL of AuNP; Spectra-, size and polarization-dependent interference fingers; and parameters of simulations.
- [29] R. Méjard, A. Verdy, M. Petit, A. Bouhelier, B. Cluzel, and O. Demichel, *ACS Photonics* **3**, 1482 (2016).
- [30] P. Biagioni, D. Brida, J. S. Huang, J. Kern, L. Duo, B. Hecht, M. Finazzi, and G. Cerullo, *Nano Lett.* **12**, 2941 (2012).
- [31] Y. Y. Cai *et al.*, *ACS Nano* **12**, 976 (2018).
- [32] A. Gliserin, S. H. Chew, S. Choi, K. Kim, D. T. Hallinan, J. W. Oh, S. Kim, and D. E. Kim, *Rev. Sci. Instrum.* **90**, 093904 (2019).
- [33] G. Hergert, J. Vogelsang, F. Schwarz, D. Wang, H. Kollmann, P. Gross, C. Lienau, E. Runge, and P. Schaaf, *Light Sci. Appl.* **6**, e17075 (2017).
- [34] Y. H. Liao, A. N. Unterreiner, Q. Chang, and N. F. Scherer, *J. Phys. Chem. B* **105**, 2135 (2001).
- [35] N. E. Karatzas and A. T. Georges, *J. Opt. Soc. Am. B* **26**, 2218 (2009).
- [36] T. Hanke, J. Cesar, V. Knittel, A. Trugler, U. Hohenester, A. Leitenstorfer, and R. Bratschitsch, *Nano Lett.* **12**, 992 (2012).
- [37] R. Mejjard, A. Verdy, M. Petit, A. Bouhelier, B. Cluzel, and O. Demichel, *ACS Photonics* **3**, 1482 (2016).
- [38] U. Delić, M. Reisenbauer, K. Dare, D. Grass, V. Vuletić, N. Kiesel, and M. Aspelmeyer, *Science* **367**, 892 (2020).
- [39] M. R. Andrews, C. G. Townsend, H.-J. Miesner, D. S. Durfee, D. M. Kurn, and W. Ketterle, *Science* **275**, 637 (1997).
- [40] T. Kovachy, P. Asenbaum, C. Overstreet, C. A. Donnelly, S. M. Dickerson, A. Sugarbaker, J. M. Hogan, and M. A. Kasevich, *Nature (London)* **528**, 530 (2015).
- [41] Y. Liu *et al.*, *Nature (London)* **543**, 229 (2017).
- [42] G. Vicidomini, P. Bianchini, and A. Diaspro, *Nat. Methods* **15**, 173 (2018).
- [43] C. Li, S. Liu, W. Wang, W. Liu, C. Kuang, and X. Liu, *J. Microsc.* **271**, 4 (2018).